ıoconjugate) for malignant

mAb	
	Collagen 4
	Ester Carbamate
	34±17 vs. 90±30*

mAb	
	Collagen 4
ıate	Ester Carbamate
	29±15 vs. 75±22*

).05

ıjugate-
Differs
ıg

ɔr ester bond (adminis-
:e evaluated in order to
ma-poor human malig-
ch human pancreatic
b-SN-38 via carbamate
ınti-CD20 mAb-SN-38
ırgeting anti-collagen 4
r antitumor activity as
mAb-SN-38 via carba-
SUIT2 tumor, the most
rgeting anti-collagen 4
was no significant dif-
b-SN-38 via carbamate
ɔf anti-collagen 4 mAb-
collagen 4 mAb-SN-38
ted that in stroma-poor
ıoconjugate should tar-
ıgated to mAb through
ıoxylesterase inside the
stroma-rich tumors, the
tumor tissue and ACA
ɔe cut gradually outside
ic immunoconjugate in

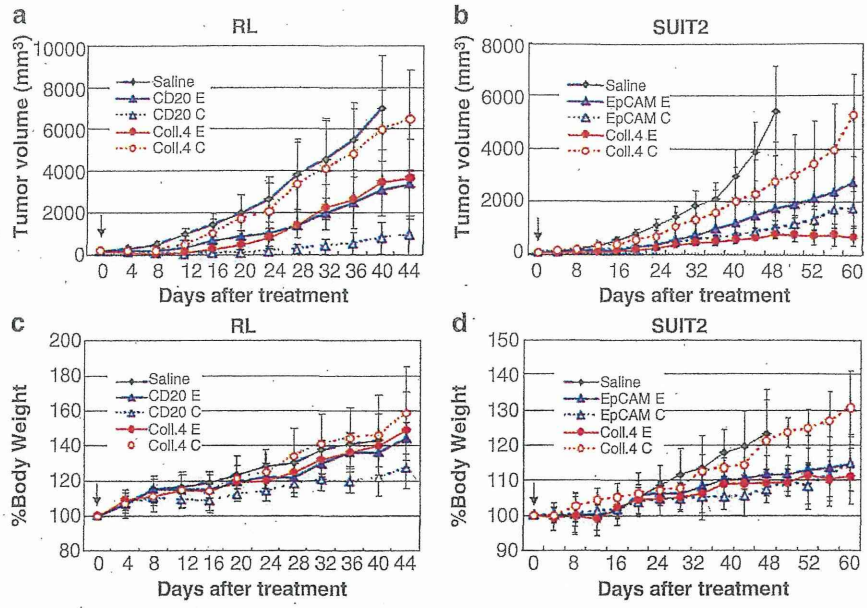

Fig. 6.12 Antitumor effects of immunoconjugates-PEG-SN-38 in the combinations of anti-cell or anti-stroma targeting, carbonate-bond or ester-bond. (**a**) (**b**) Anti-tumor activities and (**c**) (**d**) percent changes of body weight were examined. In animal models of RL (A)(C) and SUIT2 (B)(D), the 6 types of immunoconjugates (combined anti-CD20 mAb=CD20, anti-EpCAM mAb=EpCAM or anti-collagen 4 mAb=Coll.4 and ester-bond=E or carbamate-bond=C), or saline as control, were administered once at an equivalent SN-38 dose of 3 mg/kg to separate groups of mice (n=5) by intravenous bolus injection to the mice on day 0. Arrows indicate day of administration and the curves illustrate the effect of treatment on tumor size. $P < 0.0001$ (Saline vs. CD20-E or CD20-C, CD20-C vs. CD20-E, Coll.4-E or Coll.4-C in RL tumor; saline vs EpCAM-E, EpCAM-C or Coll.4-E, Coll.4-E vs. EpCAM-C or Coll.4-C, EpCAM-C vs Coll.4-C in SUIT2 tumor), $P < 0.001$ (Saline vs. Coll.4-E in RL tumor; saline vs. Coll.4-C, Coll.4-E vs. EpCAM-E in SUIT2 tumor). Bar=SD

the tumor stroma. It is remarkable that the feature of tumor stromal component influence the outcome of the two types of immunoconjugation drugs, cell-targeting mAb-PEG-SN-38 via carbamate bond, or stroma-targeting mAb-PEG-SN-38 via ester bond.

Regarding normal tissue distribution and elimination of antibodies and SN-38, there was no difference among immunoconjugates on day 7 after the administration. The dose in this study did not cause significant toxicity as shown by the change of mouse body weight (Fig. 6.12c, d). Moreover, there was no hepatotoxicity, nephrotoxicity, or bone marrow toxicity in mice treated with all three immunoconjugates as compared to controls (Fig. 6.12e). In addition, no autoimmune disease-like adverse effects such as arthritis and nephritis were observed in the administration of anti-collagen 4 mAb, whereas anti-collagen 2 mAb combined with lipopolysaccharide caused severe arthritis [49](Fig. 6.12f).

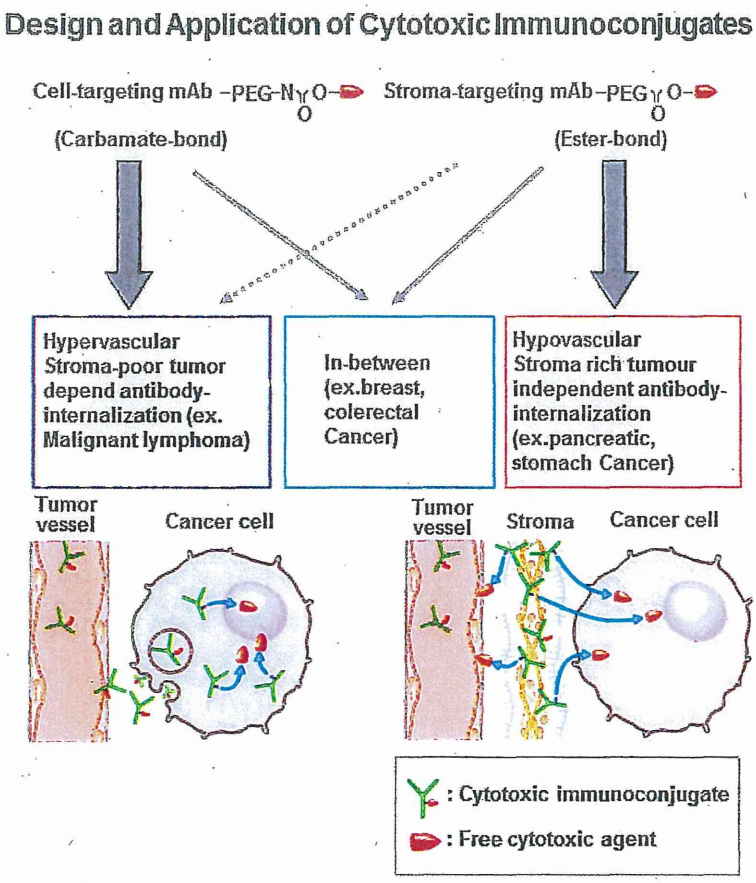

Fig. 6.13 Diagram of Immunoconjugate strategy to tumor tissue component and characteristic of cancer-cells. Design and application of cytotoxic immunoconjugates. SN-38 conjugated cell-targeting monoclonal antibody (mAb) via carbamate-bond is suitable for hypervascular, stroma-poor tumor dependent antibody-internalization. SN-38 conjugated stroma-targeting mAb via ester-bond is suitable for hypovascular, stroma-rich tumor independent antibody-internalization

In general, human cancer is classified into three types according to the tissue component. One is hypervascular stroma-poor tumor such as malignant lymphoma, the second is hypovascular stroma-rich tumor such as pancreatic cancer and stomach cancer, and the third is intermediated tumor between the two types such as breast cancer and colorectal cancer. We thus propose the new therapeutic strategy of immunoconjugates to the feature of individual tumor as tissue stromal component: (1) cell-targeting mAb conjugated with ACAs via carbamate bond for hypervascular and stroma-poor tumor and (2) stroma-targeting mAb conjugated with ACAs via ester bond for hypovascular and stroma-rich tumor, both cell-targeting immunoconjugate via carbamate bond and stroma targeting via ester bond for intermediated type of tumor [49] (Fig. 6.13).

Conclusion

Although there have b
tumors, a large body of
pivotal changes in tun
Unlike in the case of u
need to be delivered
enough to reproduce
closed space where the
agents are very strong.
the passage of time. F
human cancers possess
ing ACA-conjugated a
now concerning that cu
while ignoring pathop
ment of antitumor dru
of stromal biology wi
produce many and usef
lar diseases, and inflan

References

1. Matsumura Y, Maeda chemotherapy: mecha smancs. Cancer Res 4
2. Duncan R (2003) The
3. Maeda H, Matsumura cancer chemotherapy.
4. Courtice FC (1963) T lymphatic system. Thc
5. Iwai K, Maeda H, Kon tumor: enhanced thera
6. Tammela T, Alitalo K Cell 140:460–476
7. Gabizon AA (2001) P new form of chemothe
8. Gradishar WJ, Tjuland J (2005) Phase III trial castor oil-based paclit
9. Matsumura Y, Katao incorporating polymer
10. Duncan R (2006) P 6:688–701
11. Peer D, Karp JM, Ho emerging platform for
12. Ricart AD, Tolcher A cancer therapy. Nat Cl

oconjugates

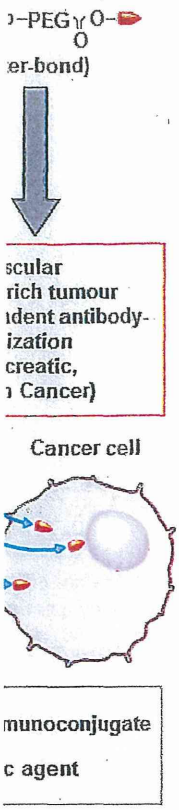

onent and characteristic of
38 conjugated cell-targeting
ascular, stroma-poor tumor
Ab via ester-bond is suitable

ccording to the tissue
malignant lymphoma,
eatic cancer and stom-
the two types such as
therapeutic strategy of
ie stromal component:
bond for hypervascu-
jugated with ACAs via
targeting immunocon-
ond for intermediated

Conclusion

Although there have been numerous reports of genetic and phenotype changes in tumors, a large body of pathological and clinical evidence indicates that there are no pivotal changes in tumor cells that distinguish them from normal dividing cells. Unlike in the case of using antibiotics against bacterial infection, therefore, ACAs need to be delivered selectively to tumor tissues and should be kept there long enough to reproduce the concentrations they reach in the Petri dish, which is a closed space where the cytocidal effects of any ACAs including molecular targeting agents are very strong. In the body, however, administered ACAs are cleared with the passage of time. Furthermore, as described in the main part of this topic, most human cancers possess abundant stroma that hinders the penetration of DDS including ACA-conjugated antibodies specific to surface antigens on cancer cells. We are now concerning that current studies mainly based on molecular and cellular biology while ignoring pathophysiology and pharmacology may be leading the development of antitumor drugs in the wrong direction. The present discovery by a hybrid of stromal biology with organic chemistry may open a new field of science and produce many and useful treatment modalities in the area of oncology, cardiovascular diseases, and inflammation.

References

1. Matsumura Y, Maeda H (1986) A new concept for macromolecular therapeutics in cancer chemotherapy: mechanism of tumoritropic accumulation of proteins and the antitumor agent smancs. Cancer Res 46:6387–6392
2. Duncan R (2003) The dawning era of polymer therapeutics. Nat Rev 2:347–360
3. Maeda H, Matsumura Y (2011) EPR effect based drug design and clinical outlook for enhanced cancer chemotherapy. Adv Drug Deliv Rev 63:129–192
4. Courtice FC (1963) The origin of lipoprotein in lymph. In: Meyersen HS (ed) Lymph and the lymphatic system. Thomas CC, Springfield, IL, pp 89–126
5. Iwai K, Maeda H, Konno T (1984) Use of oily contrast medium for selective drug targeting to tumor: enhanced therapeutic effect and X-ray image. Cancer Res 44:2115–2121
6. Tammela T, Alitalo K (2010) Lymphangiogenesis: molecular mechanisms and future promise. Cell 140:460–476
7. Gabizon AA (2001) Pegylated liposomal doxorubicin: metamorphosis of an old drug into a new form of chemotherapy. Cancer Invest 19:424–436
8. Gradishar WJ, Tjulandin S, Davidson N, Shaw H, Desai N, Bhar P, Hawkins M, O'Shaughnessy J (2005) Phase III trial of nanoparticle albumin-bound paclitaxel compared with polyethylated castor oil-based paclitaxel in women with breast cancer. J Clin Oncol 23:7794–7803
9. Matsumura Y, Kataoka K (2009) Preclinical and clinical studies of anticancer agent-incorporating polymer micelles. Cancer Sci 100:572–579
10. Duncan R (2006) Polymer conjugates as anticancer nanomedicines. Nat Rev Cancer 6:688–701
11. Peer D, Karp JM, Hong S, Farokhzad OC, Margalit R, Langer R (2007) Nanocarriers as an emerging platform for cancer therapy. Nat Nanotechnol 2:751–760
12. Ricart AD, Tolcher AW (2007) Technology insight: cytotoxic drug immunoconjugates for cancer therapy. Nat Clin Pract Oncol 4:245–255

13. Doronina SO, Toki BE, Torgov MY, Mendelsohn BA, Cerveny CG, Chace DF, DeBlanc RL, Gearing RP, Bovee TD, Siegall CB, Francisco JA, Wahl AF, Meyer DL, Senter PD (2003) Development of potent monoclonal antibody auristatin conjugates for cancer therapy. Nat Biotechnol 21:778–784
14. Wu AM, Senter PD (2005) Arming antibodies: prospects and challenges for immunoconjugates. Nat Biotechnol 23:1137–1146
15. Doronina SO, Bovee TD, Meyer DW, Miyamoto JB, Anderson ME, Morris-Tilden CA, Senter PD (2008) Novel peptide linkers for highly potent antibody-auristatin conjugate. Bioconjug Chem 19:1960–1963
16. Verma S et al (2012) Trastuzumab emtansine for HER2-positive advanced breast cancer. N Engl J Med 367(19):1783–1791
17. Koenders PG, Peters WH, Wobbes T, Beex LV, Nagengast FM, Benraad TJ (1992) Epidermal growth factor receptor levels are lower in carcinomatous than in normal colorectal tissue. Br J Cancer 65:189–192
18. Messersmith W, Oppenheimer D, Peralba J, Sebastiani V, Amador M, Jimeno A, Embuscado E, Hidalgo M, Iacobuzio-Donahue C (2005) Assessment of epidermal growth factor receptor (EGFR) signaling in paired colorectal cancer and normal colon tissue samples using computer-aided immunohistochemical analysis. Cancer Biol Ther 4:1381–1386
19. Hayden EC (2006) Cancer complexity slows quest for cure. Nature 455:148
20. Heng HHQ, Bremer SW, Stevens JB, Ye KJ, Liu G, Ye CJ (2009) Genetic and epigenetic heterogeneity in cancer: a genome-centric perspective. J Cell Physiol 220:538–547
21. Collins BE, Blixt O, Han S, Duong B, Li H, Nathan JK, Bovin N, Paulson JC (2006) High-affinity ligand probes of CD22 overcome the threshold set by cis ligands to allow for binding, endocytosis, and killing of B cells. J Immunol 177:2994–3003
22. Schmidt MM, Thurber GM, Wittrup KD (2008) Kinetics of anti-carcinoembryonic antigen antibody-internalization: effects of affinity, bivalency, and stability. Cancer Immunol Immunother 57:1879–1890
23. Burke PJ, Senter PD, Meyer DW, Miyamoto JB, Anderson M, Toki BE, Manikumar G, Wani MC, Kroll DJ, Jeffrey SC (2009) Design, synthesis, and biological evaluation of antibody-drug conjugates comprised of potent camptothecin analogues. Bioconjug Chem 20:1242–1250
24. Coyne CP, Jones T, Pharr T (2011) Synthesis of a covalent gemcitabine-(carbamate)-[anti-HER2/neu] immunochemotherapeutic and its cytotoxic anti-neoplastic activity against chemotherapeutic-resistant SKBr-3 mammary carcinoma. Bioorg Med Chem 19:67–76
25. Dvorak HF (1986) Tumors: wounds that do not heal. Similarities between tumor stroma generation and wound healing. N Engl J Med 315:1650–1659
26. Minchinton AI, Tannock IF (2006) Drug penetration in solid tumors. Nat Rev Cancer 6:583–592
27. Trédan O, Galmarini CM, Patel K, Tannock IF (2007) Drug resistance and the solid tumor microenvironment. J Natl Cancer Inst 99:1441–1454
28. Ghajar CM, Bissell MJ (2008) Extracellular matrix control of mammary gland morphogenesis and tumorigenesis: insights from imaging. Histochem Cell Biol 130:1105–1118
29. Yasunaga M, Manabe S, Tarin D, Matsumura Y (2011) Cancer-stroma targeting therapy by cytotoxic immunoconjugate bound to the collagen 4 network in the tumor tissue. Bioconjug Chem 22:1776–1783
30. Yasunaga M, Manabe S, Matsumura Y (2011) New concept of cytotoxic immunoconjugate therapy targeting cancer-induced fibrin clots. Cancer Sci 102:1396–1402
31. Maeda H, Matsumura Y, Kato H (1988) Purification and identification of (hydroxyprolyl^3)-bradykinin in ascitic fluid from a patient with gastric cancer. J Biol Chem 263:16051–16054
32. Matsumura Y, Kimura M, Yamamoto T, Maeda H (1988) Involvement of the kinin-generating cascade and enhanced vascular permeability in tumor tissue. Jpn J Cancer Res 79:1327–1334
33. Senger DR, Galli SJ, Dvorak AM, Peruzzi CA, Harvey VS, Dvorak HF (1983) Tumor cells secret a vascular permeability factor that promotes accumulation of ascites fluid. Science 21:983–985

34. Ferrara N, Hillan KJ bevacizumab, an anti-V
35. Dvorak HF, Rickles F Clowes AW, George JN clinical practice, 5th ed
36. Trousseau A (1865) Pe
37. Stein PD, Beemath A, thromboembolism in p
38. Naito S, von Eschenba of human renal cell car 78:377–385
39. Fallowfield ME (1989) J Cancer Clin Oncol 2
40. Ellis LM, Fidler IJ (20 16:974–975
41. Hawighorst T, Velasco M (2001) Thrombospo anti-tumor defense me
42. Rehlaender BN, Cho M
43. Bhowmick NM, Neils progression. Nature 43
44. Alderton GK (2010) T 10:162–163
45. Matsumura Y (2012) 64:710–719
46. Iwamura T, Katsuki T, cancer cell line (SUIT- Jpn J Cancer Res 78:5
47. Senter PD, Beam KS, xylesterases for the ac Chem 12:1074–1080
48. Pommier Y (2006) To 6:789–802
49. Yasunaga M, Manabe depending on a quantit

G, Chace DF, DeBlanc RL,
eyer DL, Senter PD (2003)
tes for cancer therapy. Nat

allenges for immunoconju-

3, Morris-Tilden CA, Senter
statin conjugate. Bioconjug

ve advanced breast cancer.

enraad TJ (1992) Epidermal
normal colorectal tissue. Br

r M, Jimeno A, Embuscado
rmal growth factor receptor
ue samples using computer-
386
e 455:148
Genetic and epigenetic het-
220:538–547
N, Paulson JC (2006) High-
ligands to allow for binding,

i-carcinoembryonic antigen
stability. Cancer Immunol

ki BE, Manikumar G, Wani
evaluation of antibody-drug
ug Chem 20:1242–1250
ncitabine-(carbamate)-[anti-
neoplastic activity against
Med Chem 19:67–76
between tumor stroma gen-

l tumors. Nat Rev Cancer

istance and the solid tumor

nmary gland morphogenesis
30:1105–1118
stroma targeting therapy by
the tumor tissue. Bioconjug

cytotoxic immunoconjugate
6–1402
ication of (hydroxyprolyl^3)-
ol Chem 263:16051–16054
ment of the kinin-generating
J Cancer Res 79:1327–1334
orak HF (1983) Tumor cells
on of ascites fluid. Science

34. Ferrara N, Hillan KJ, Gerber HP, Novotny W (2004) Discovery and development of bevacizumab, an anti-VEGF antibody for treating cancer. Nat Rev Drug Discov 3:391–400
35. Dvorak HF, Rickles FR (2006) Malignancy and hemostasis. In: Colman RW, Marder VJ, Clowes AW, George JN, Goldharber SZ (eds) Hemostasis and thrombosis: basic principles and clinical practice, 5th edn. Lippincott Williams & Wilkins, Philadelphia, PA, pp 851–873
36. Trousseau A (1865) Pegmasia alba dolens, vol 3. Balliere JB et Fils, Paris
37. Stein PD, Beemath A, Meyers FA, Skaf E, Sanchez J, Olson RE (2006) Incidence of venous thromboembolism in patients hospitalized with cancer. Am J Med 119:60–68
38. Naito S, von Eschenbach AC, Fidler IJ (1987) Different growth pattern and biologic behavior of human renal cell carcinoma implanted into different organs of nude mice. J Natl Cancer Inst 78:377–385
39. Fallowfield ME (1989) Blood flow distribution within transplantable tumors in the mouse. Eur J Cancer Clin Oncol 25:1683–1688
40. Ellis LM, Fidler IJ (2010) Finding the tumor copycat. Therapy fails, patients don't. Nat Med 16:974–975
41. Hawighorst T, Velasco P, Streit M, Hong YK, Kyriakides TR, Brown LF, Bornstein P, Detmar M (2001) Thrombospondin-2 plays a protective role in multistep carcinogenesis: a novel host anti-tumor defense mechanism. EMBO J 20:2631–2640
42. Rehlaender BN, Cho MJ (1998) Antibodies as carrier proteins. Pharm Res 15:1652–1656
43. Bhowmick NM, Neilson EG, Moses HL (2004) Stromal fibroblast in cancer initiation and progression. Nature 432:332–337
44. Alderton GK (2010) Tumor microenvironment: macrophages lead the way. Nat Rev Cancer 10:162–163
45. Matsumura Y (2012) Cancer stromal targeting (CAST) therapy. Adv Drug Deliv Rev 64:710–719
46. Iwamura T, Katsuki T, Ide K (1987) Establishment and characterization of a human pancreatic cancer cell line (SUIT-2) producing carcinoembryonic antigen and carbohydrate antigen 19-9. Jpn J Cancer Res 78:54–62
47. Senter PD, Beam KS, Mixan B, Wahl AF (2001) Identification and activities of human carboxylesterases for the activation of CPT-11, a clinically approved anticancer drug. Bioconjug Chem 12:1074–1080
48. Pommier Y (2006) Topoisomerase I inhibitors: camptothecins and beyond. Nat Rev Cancer 6:789–802
49. Yasunaga M, Manabe S, Tarin D, Matsumura Y (2013) Tailored immunoconjugate therapy depending on a quantity of tumor stroma. Cancer Sci 104:231–237

SCIENTIFIC REPORTS

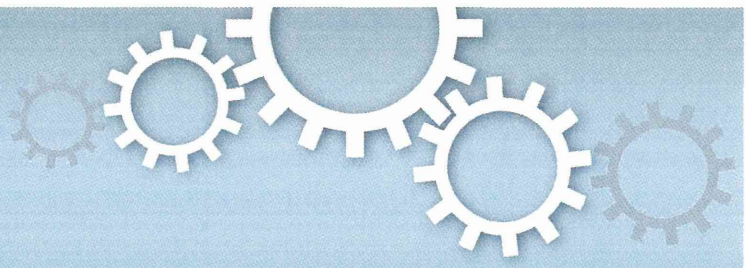

OPEN

SUBJECT AREAS:
PHARMACOKINETICS
PHARMACODYNAMICS
DRUG DELIVERY
BIOCHEMICAL ASSAYS

Received
23 May 2013

Accepted
10 October 2013

Published
25 October 2013

Correspondence and requests for materials should be addressed to Y.M. (yhmatsum@east.ncc.go.jp)

The significance of microscopic mass spectrometry with high resolution in the visualisation of drug distribution

Masahiro Yasunaga[1], Masaru Furuta[2], Koretsugu Ogata[2], Yoshikatsu Koga[1], Yoshiyuki Yamamoto[1], Misato Takigahira[1] & Yasuhiro Matsumura[1]

[1]Division of Therapeutics Development, Research Center for Innovative Oncology, National Cancer Center Hospital East, 6-5-1 Kashiwanoha, Kashiwa, Chiba 277-8577, Japan, [2]Analytical & Measuring Instruments Division, Shimadzu Corporation, 1, Nishinokyo-Kuwabaracho, Nakagyo-ku, Kyoto 604-8511, Japan.

The visualisation and quantitative analysis of the native drug distribution in a pre-clinical or clinical setting are desirable for evaluating drug effects and optimising drug design. Here, using matrix-assisted laser desorption ionisation imaging mass spectrometry (MALDI-IMS) with enhanced resolution and sensitivity, we compared the distribution of a paclitaxel (PTX)-incorporating micelle (NK105) with that of PTX alone after injection into tumour-bearing mice. We demonstrated optically and quantitatively that NK105 delivered more PTX to the tumour, including the centre of the tumour, while delivering less PTX to normal neural tissue, compared with injection with PTX alone. NK105 treatment yielded a greater antitumour effect and less neural toxicity in mice than did PTX treatment. The use of high-resolution MALDI-IMS may be an innovative approach for pharmacological evaluation and drug design support.

Advances in our understanding of cancer at the cellular and molecular levels have promoted the development of new drugs[1,2]. Pharmacokinetic (PK) and pharmacodynamic (PD) studies are very important to evaluate the efficacy and toxicity of new drugs as well as to optimise drug design. For these purposes, tissue homogenate samples are generally analysed by high-performance liquid chromatography (HPLC) or liquid chromatography mass spectrometry (LC-MS)[3]. For the development of anticancer drugs (ACAs), including molecular targeting agents, precise chemical modulation is needed because the small differences between cancer cells and their host cells creates a narrow therapeutic window. In addition, clinical human cancer tissues generally exhibit abundant and versatile stroma, which is the result of the process of tumour cell invasion into tumour vessels, haemorrhage, fibrin clot formation, and replacement with collagen tissues and non-malignant stromal cells. Therefore, it is very important to consider the delivery of ACAs to cancer tissues and their distribution to target cancer cells within this heterogeneous tumour microenvironment. Furthermore, the drug distribution within normal tissues, particularly vital organs, should also be evaluated because ACAs frequently cause adverse effects[4]. A large body of clinical evidence has revealed that neoadjuvant chemotherapy is useful for a variety of solid tumours. The tissue excised during surgery or endoscopic biopsy can be used to investigate drug distribution[5,6]. Thus, a convenient method for evaluating the distribution of clinically used native (non-radiolabeled or non-chemically modified) drugs is urgently required.

Matrix-assisted laser desorption ionisation imaging mass spectrometry (MALDI-IMS) has been developed for the investigation of the distribution of molecules such as small peptides, drugs, and their metabolites[7–12]. Moreover, MALDI-IMS can be used to evaluate numerous molecules in a single measurement without a specialised probe[7–12]. Therefore, this method enables the observation of a drug directly within tissue with the distinction between the original compound and its metabolites.

We have developed a mass microscopy method in which a microscope is coupled with a high-resolution atmospheric pressure-laser desorption/ionisation and quadruple ion trap time-of-flight (TOF) analyser. In this study, we investigated the ability of our mass microscopy technique to visualise the tissue distribution of unlabelled ACA and its micellar formulation and obtain precise regional information about the drug distribution in a specific anatomical area.

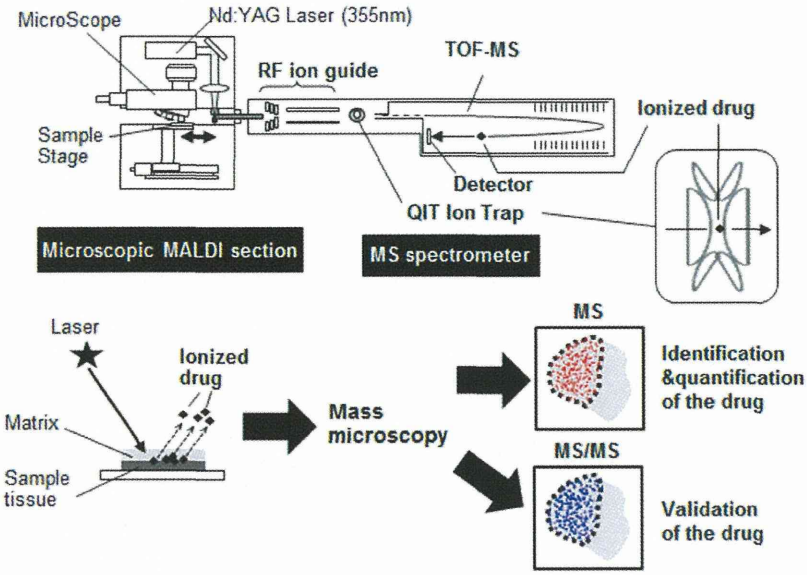

Figure 1 | Drug imaging system. A schematic illustration of the drug imaging system. The matrix-coated drug sample is ionised and then separated on the basis of its *m/z*. Images from MS or MS/MS analysis are recorded.

Results

The drug imaging system and its application in PTX analysis on the MALDI target. A schematic representation of our drug imaging system is shown in Fig. 1. Imaging data were acquired using a mass microscope. In the analysis, mass spectrometry (MS) and tandem mass spectrometry (MS/MS) were used for quantification and validation, respectively (Fig. 1).

Paclitaxel (PTX) is a mitotic inhibitor and an ACA that is used to treat various cancers. However, PTX is associated with peripheral neuropathy, a serious adverse affect[13]. NK105, a PTX-incorporating micelle, was developed to address this limitation of PTX[14–17]. On the basis of the enhanced permeability and retention (EPR) effect[17–20], NK105 can be selectively delivered to a tumour, resulting in an enhanced antitumour effect and the minimisation of adverse effects, including peripheral neuropathy. The high efficacy and low toxicity of NK105 have been demonstrated in both preclinical and clinical studies[14–17]. Although the administered drug content per tissue weight can be determined by conventional HPLC or LC-MS, the detailed drug distribution within the tumour and normal tissue has not been examined. Therefore, we used our drug imaging system to evaluate the difference in the distribution of NK105 and free PTX within tumour and normal peripheral neuronal tissue.

Antitumour activity and visualisation of PTX and NK105 distribution within the tumour with MS analysis. NK105 or PTX was administered at a PTX equivalent dose of 50 mg/kg/day to mice bearing BxPC3 pancreatic cancer xenografts on days 0, 4, and 8. NK105 showed significantly higher antitumour activity than the control (saline) and free PTX (Fig. 2a). To confirm the correlation of the distribution with the antitumour effect, the corresponding tumour sections were subjected to MALDI-IMS. A drug signal originating from PTX was detected in the tumours at 15 min and 1 h after the administration of PTX, but this signal decreased at 6 h and was below the limit of detection by 24 h (Fig. 2b). By contrast, the signal originating from the PTX released from NK105 (rPTX) following the accumulation of NK105 in the tumour was detected at 15 min as well as at 1, 24, 48, and 72 h after the administration of NK105. The signal intensity was greatest at 24 h (Fig. 2c). Tissue sections serial to those for MALDI-MS were also quantified by LC-MS (Fig. 2d, e), the results of which correlated with the drug imaging results (Fig. 2b–e). The data did not contradict previous data obtained by HPLC[14]. The results of the MALDI-MS analysis demonstrate that significant levels of PTX were present in the tumour clusters, including within the centre of the tumour tissue.

Validation of the PTX and NK105 distribution within tumour tissue by MS/MS analysis. Validation of the PTX content in each sample was performed in MS/MS mode. A structural diagram and the MS/MS fragmentation pattern (FP) of PTX are shown in Fig. 3a and b, respectively. According to the MS/MS-FP, *m/z* 607.19, which was selected as a PTX-specific fragment peak (Fig. 3c), was observed at a higher level in the tumour tissue sample at 1 h after PTX injection than at 1 h after NK105 injection (Fig. 3d, e).

Peripheral neurotoxicity and visualisation of the PTX and NK105 distribution by MS analysis. Next, a mechanical stress test that measured the degree of peripheral neurotoxicity demonstrated that the mice in the PTX treatment group exhibited a significantly stronger hypersensitive reaction to the mechanical stress test than those in the control and NK105 treatment groups (Fig. 4a). To confirm the correlation of the distribution with the abnormal neurological reaction, we also applied MALDI-IMS and examined the distribution of PTX in peripheral neural tissue at 30 min, 1 h, and 24 h after administration. The signals surrounding and inside the nerve were lower after NK105 injection than after PTX injection (Fig. 4b, c). LC-MS analysis of the neural samples revealed that the concentration of rPTX after NK105 injection was also lower than that after PTX injection (Fig. 4d).

Discussion

Conventional MALDI-IMS was expected to aid in the analysis of the global distribution of drugs within tissue. However, its application has been limited for a variety of reasons, including its limited resolution[7,8]. Recent progress in MALDI-IMS analysis, including the new features of our instrument, have achieved a MALDI-IMS resolution of 10 μm or less, which is advantageous for evaluating the drug distribution in specific cells or areas of interest within tissues[9–12]. The improved resolution also allows an IMS image to be overlaid on an optical image of the same sample. In fact, we were able to distinguish the nerve component from the surrounding tissue and evaluate the specific distribution of PTX in the region.

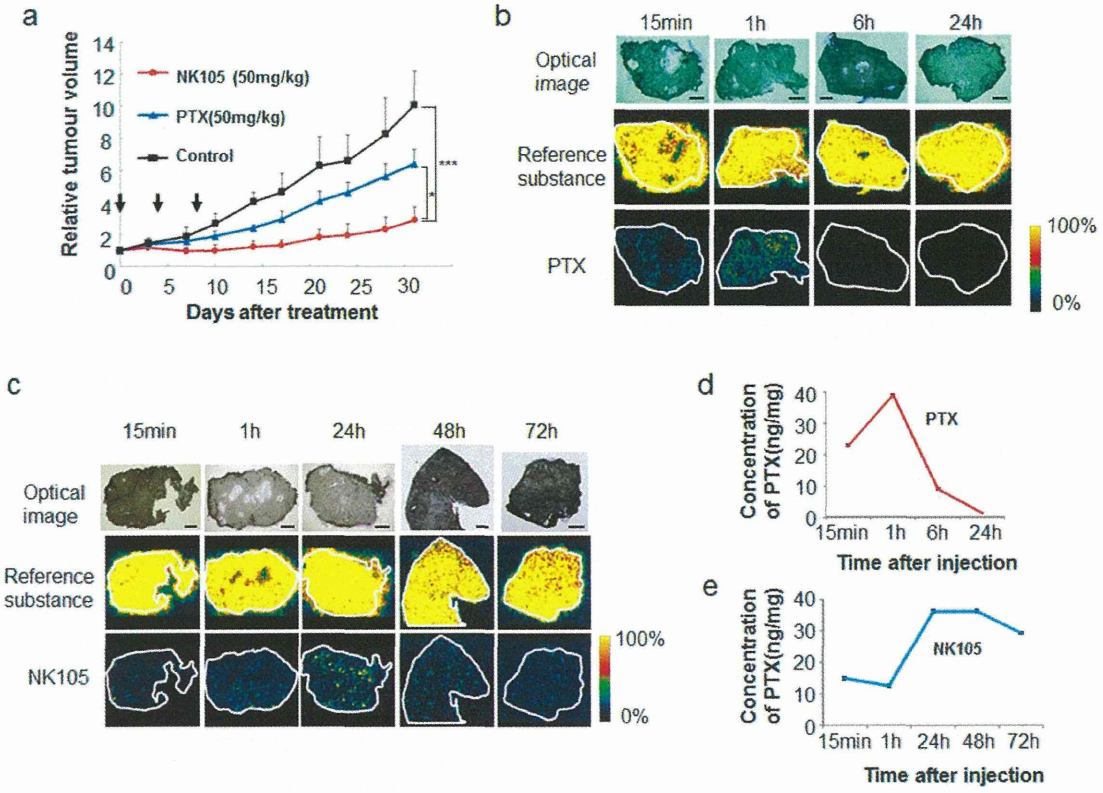

Figure 2 | Antitumour activity and visualisation of PTX and NK105 distribution with MS analysis. (a) Antitumour activity was examined in an animal model with BXPC3 xenografts. NK105, PTX, or saline (as a control) was administered at a PTX equivalent dose of 50 mg/kg on days 0, 4, and 8. *$P < 0.05$ (PTX vs. NK105), ***$P < 0.001$ (saline vs. NK105). Bar = SD. (b)(c) Imaging of PTX within the tumour was performed after PTX (b) or NK105 (c) administration at a dose of 100 mg/kg. The upper, middle, and lower columns display the optical images, reference substance (an arbitrary signal of *m/z* 824.6), and PTX (specific signal of *m/z* 892.3 $[M + K]^+$), respectively. Bar, 1 mm. (d)(e) LC-MS analysis of the PTX concentration in the tumours treated by PTX (d) or NK105 (e). Tissue sections serial to those shown in (b) and (c).

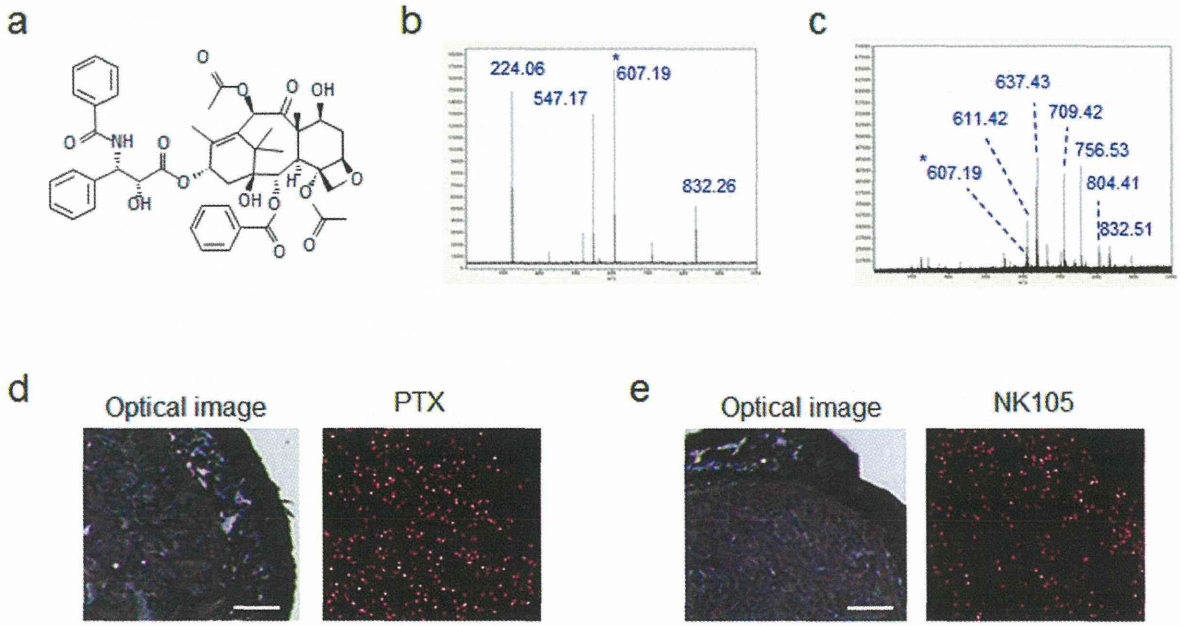

Figure 3 | Validation of the PTX and NK105 distribution within the tumour tissues by MS/MS analysis. (a) The structure of PTX is shown. (b) (c) The PTX-specific MS/MS fragments at *m/z* 224.06, 547.17, 607.19, and 832.26 are shown in (b). The fragment pattern from MS/MS analysis of the tumour tissue sample is shown in (c). (d) (e) Images obtained by optical microscopy (left) and by MS/MS analysis of PTX (*m/z* 607.19*) (right) in tumours treated with PTX (d) or NK105 (e) at 1 h after injection. Bar, 500 μm.

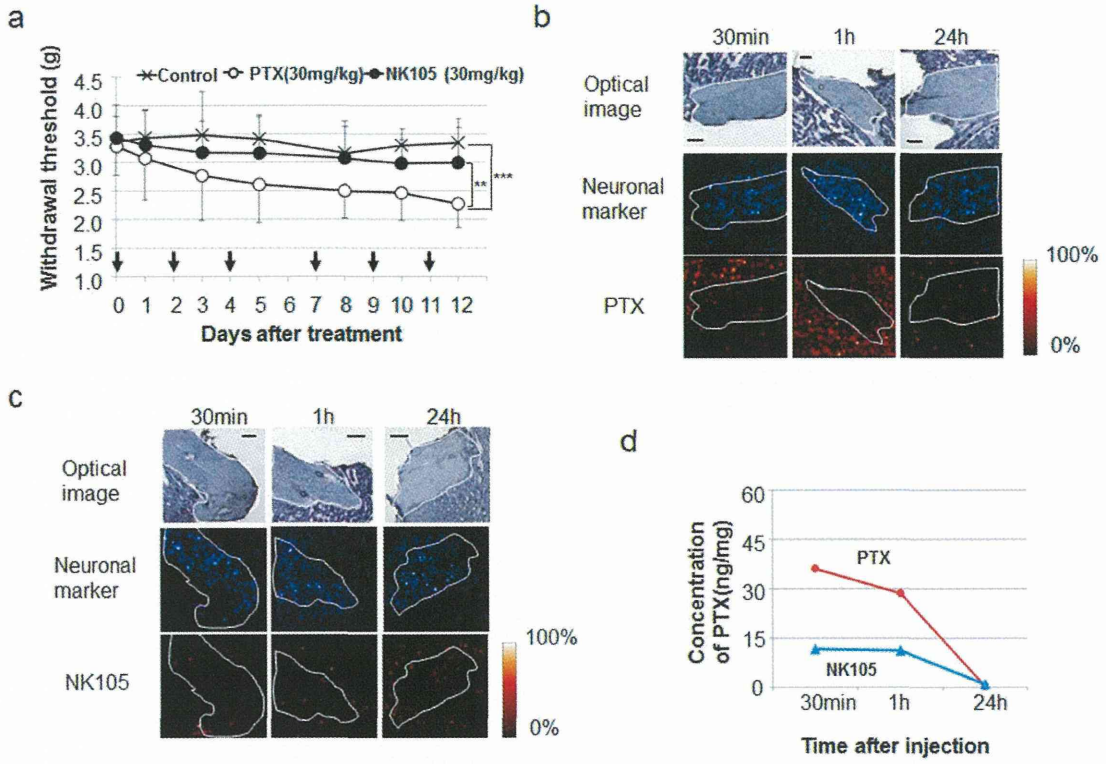

Figure 4 | Peripheral neurotoxicity and visualisation of PTX and NK105 distribution by MS analysis. (a) Mechanical sensory stress was assayed in an animal model of PTX-induced peripheral neuropathy. NK105, PTX, or saline was administered at 30 mg/kg on days 0, 2, 4, 7, 9, and 11. $^{**}P < 0.01$ (PTX vs. NK105), $^{***}P < 0.001$ (saline vs. PTX). Bar = SD. (b) (c) PTX within neuronal tissue was imaged after PTX (b) or NK105 (c) administration at a dose of 50 mg/kg. The upper, middle, and lower columns show the optical images, a neuronal marker (sphingomyelin-specific signal of 851.6 *m/z*), and PTX (specific signal of *m/z* 892.3 $[M + K]^+$), respectively. The neuronal area is delineated by a white line. Bar, 200 μm. (d) Analysis of the PTX concentration by LC-MS. Tissue sections serial to those shown in (b) and (c).

Tissue samples should be frozen without liquid solution to avoid the diffusion or loss of the drug from the tissue to the solution. For efficient ionisation in the present study, the sample was coated with a sufficient quantity of matrix by spraying. 2,5-Dihydroxybenzoic acid (DHB) was selected as the matrix to facilitate the efficient ionisation of the drug. We are now attempting to use several other matrix materials to enhance the sensitivity of our MALDI-IMS technique. Moreover, we used a combination of MS and MS/MS for the imaging analysis. In the MS analysis, accurate quantification of PTX was demonstrated in vivo. In the MS/MS analysis, the presence of PTX was validated by a fragment-specific signal at 607.19 *m/z*, which does not overlap with any other signals. The combination of MS and MS/MS thus facilitates the accurate evaluation of the drug-originated signal by distinguishing the drug signal from endogenous metabolites with a similar m/z.

In this report, MALDI-IMS demonstrated that NK105 successfully delivered a large amount of the PTX payload within the tumour tissue after NK105 injection compared with PTX injection alone. More importantly, the precise localisation and levels of PTX within the tumour tissue were visualised and quantified due to the high resolution of the MALDI-IMS technique. The obtained data did not contradict our MS data or previous data obtained by conventional pharmacological analysis using HPLC[14]. Thus, our data demonstrated that the antitumour activity of NK105 is superior to that of PTX alone. In addition, the peripheral neurotoxicity of NK105 was significantly lower than that of PTX, consistent with the MALDI-IMS data. In fact, in a phase 2 clinical trial of NK105 in patients with previously treated advanced stomach cancer, only one of the 56 patients (1.8%) who entered the trial experienced grade 3 peripheral neuropathy[16]. Phase 2 trials of other PTX formulations, including Abraxane and conventional PTX, have demonstrated that the incidence of grade 3 or 4 peripheral neuropathy is greater than 10%[21,22]. A phase 3 clinical trial of NK105 vs. PTX is now underway, which may elucidate the clinical significance of this micellar drug delivery system (DDS).

Although many studies have indicated that NK105 accumulates selectively in tumour tissue compared to PTX by HPLC or LC-MS analysis, whether NK105 could deliver PTX to cancer-cell clusters within the tumour tissue was unknown. Cancer tissue is heterogeneous and consists not only of cancer cells but also of abundant tumour stroma, the latter of which can act as a barrier against macromolecules, including NK105[23,24]. In the present study, significant levels of PTX, even in the core of the tumour tissue, were observed following NK105 administration, and the NK105 was retained for a long period of time.

Low molecular weight (LMW) ACAs, including molecular targeting agents, can easily extravasate from normal blood vessels and cause various adverse effects. DDS drugs such as NK105, which exhibit low short-term accumulation in normal tissues that lack the EPR effect, can minimise this drug toxicity. Our data clearly demonstrate that the distribution of rPTX from NK105 in the peripheral nerve and surrounding tissues was quite low compared with PTX alone. These observations support the low incidence of peripheral neuropathy when PTX is administered as NK105.

This is the first report describing the precise distribution of a DDS drug by MSI, a new technique developed by our lab and others. Notably, we successfully visualise and quantified the distribution of a non-radiolabeled and non-chemically modified drug in various frozen tissue slices microscopically. In addition to PTX, we have successfully visualised other anticancer agents, including SN-38,

epirubicin, and monomethyl auristatin E (MMAE) (data not shown). This success indicates that the MALDI-IMS technique can be applied to clinical biopsy specimens or surgically resected tissues after neo-adjuvant chemotherapy. In addition, the data obtained by MALDI-IMS can be utilised to facilitate drug design.

Methods

Cells and reagents. The human pancreatic cancer cell line BxPC3 was purchased from the American Type Culture Collection and maintained in DMEM (Sigma, St. Louis, MO) supplemented with 10% foetal bovine serum (Tissue Culture Biologicals, CA), penicillin, streptomycin, and amphotericin B (Sigma) at 5% CO_2 and 37°C. NK105, a PTX-incorporating 'core-shell-type' polymeric micellar nanoparticle, was supplied by Nippon Kayaku Co. Ltd. (Tokyo, Japan). The weight-average diameter of the nanoparticles was approximately 85 nm, ranging from 20 to 430 nm. PTX was purchased from Tokyo Chemical Industry Co. (Tokyo, Japan).

Drug imaging by mass microscopy. IMS analysis was performed using an atmospheric pressure (AP) MALDI-IT-TOF mass spectrometer (prototype Mass Microscope; Shimadzu)[25].

To prepare tissue samples, the tumour and sciatic nerve with surrounding tissue were surgically removed from a xenograft model at 15 min, 30 min, 1 h, or 24 h after drug administration (50 or 100 mg/kg). Samples wrapped in gauze were frozen in dry ice powder. The samples were then sectioned at a thickness of 10 μm and transferred to an indium tin oxide-coated glass slide (Sigma). The tissue section was dried (with no washing step) before matrix coating.

For the application of the matrix onto the tissue slide, 30 and 50 mg/ml of DHB in 50% methanol and 0.1% trifluoroacetic acid were used. The 30 mg/ml DHB solution (0.4 ml) was sprayed twice, and then the 50 mg/ml (0.4 ml) solution was sprayed once with a 0.2-mm nozzle calibre airbrush (Procon Boy FWA Platinum; Mr. Hobby, Tokyo, Japan); each spraying step was completed over 5 min. During spraying, the distance between the nozzle and the tissue surface was maintained at 15 cm to keep the surface dry.

IMS analyses were performed in positive-ion mode within a mass range of *m/z* 720–920 for PTX, with a spatial resolution of 30 μm. The laser was irradiated at 40 shots/spectrum at a frequency of 400 Hz, and the power was set to 60–65% using the Mass Microscope operation software. PTX distribution mapping was performed in BioMap (Novartis, Basel, Switzerland) using the *m/z* 892.3 ($[M + K]^+$) signal because the $[M + K]^+$ signal showed more sensitive mass spectra than did the $[M + H]^+$ and $[M + Na]^+$ signals. The uniformly distributed *m/z* 824.6 ion (corresponding to cerebrosides (42 : 6) + Na) in tumour sections and *m/z* 851.6 ion (sphingomyelin (d18 : 1/24 : 1) + K) in neuronal tissue were used as internal controls to correct the PTX signal intensity.

MS/MS analysis of PTX (*m/z* 892.3) was performed with the CID function of the quadruple ion trap cell on the Mass Microscope. The *m/z* 607.19 fragment ion was generated on the tissue. This ion was also observed for the authentic PTX as the derivative and was used for MS/MS imaging of the drug. The instrument conditions for MS/MS imaging were identical to those used for the MS mapping described above, but the spatial resolution was 15 μm, and the laser power was 50%.

Animal model. *Antitumour activity.* Female BALB/c nude mice (5 weeks old) and DBA/2N mice (8 weeks old) were purchased from SLC Japan (Shizuoka, Japan). The nude mice were inoculated subcutaneously in the flank with 1×10^6 BxPC3 cells. The length (L) and width (W) of the tumour masses were measured every 3 to 4 days, and the tumour volume was calculated using the following formula: $(L \times W^2)/2$. When the mean tumour volume reached approximately 300 mm^3, the mice were randomly assigned to groups of five. Drugs (50 mg/kg) were administered on days 0, 4, and 8 by injection into the mouse tail vein.

Peripheral neuropathy. To investigate the neurotoxicity induced by PTX and NK105, we designed the following experimental scheme: The development of nocifensive responses to mechanical stimuli was assessed in the mice (ref). Six-week-old female DBA/2N mice were randomly assigned to one of three groups, and their baseline nocifensive responses were measured. We confirmed that the mean latency was statically identical between the groups. The mice were then administered a dose of 30 mg/kg PTX or 30 mg/kg NK105 on days 0, 2, and 4 every week for 2 weeks, for a total of 6 injections (n = 10). Control mice were injected with 5% dextrose solution on the same schedule. After a total of 6 administrations, the mice were tested for transitional changes in their nocifensive responses. Mechanical allodynia was assessed by measuring the latency of paw withdrawal in response to noxious mechanical stimuli using a Dynamic Plantar Aesthesiometer (Ugo Basile, Varese, Italy). The mice were placed on a wire mesh floor in individual Plexiglas cages and were allowed to acclimate for approximately 1 h, during which exploratory and grooming activity was completed. The mechanical stimulus was applied to the plantar aspect of the hind paw using a 2-mm-diameter metal filament. The force was automatically increased at a fixed rate (0–5 g, 0.25 g/sec) until the mouse withdrew its paw. The analysis of paw withdrawal responses was repeated 4 times at 10-sec intervals. The paw withdrawal threshold (g) was determined from the average of the four measurements. None of the mice in this assay were inoculated with tumour cells.

All animal procedures and experiments were approved by Committee for Animal Experimentation of the National Cancer Centre, Tokyo Japan.

These guidelines meet the ethical standards required by law and comply with the guidelines for the use of experimental animals in Japan.

Statistical analysis was performed using analysis of variance (ANOVA) with Tukey's multiple comparison tests.

LC-MS. For LC-MS, several sections immediately adjacent to the sections for IMS imaging were serially collected into a vial, and the drug was extracted into acetonitrile by vortexing. The samples were analysed with a Liquid Chromatograph Mass Spectrometer LCMS-8040 (Shimadzu Corp.). A Kinetex 2.6 μm C18 100A (100 × 2.1 mm) analytical column was used. The injection volume was 1 μl, and the flow rate was 0.5 ml/min. (A) Acetonitrile and (B) 0.1% (w/v) formic acid solution were used as the mobile phases. The mobile phase was introduced into the spectrometer via electrospray ionisation in positive ion mode under multiple reaction monitoring (MRM) conditions. In terms of the gradient, acetonitrile was conducted at 50% (B) for the first 1.5 min, increased to 100% for 0.25 min, and subsequently decreased back to 50% for 1.25 min. The PTX quantification was performed with the precursor *m/z* 854.45 ion, and the standard curve generated using the product *m/z* 104.95 ion was used. The data were collected in triplicate experiments.

1. Chin, L. & Gray, J. W. Translating insights from the cancer genome into clinical practice. *Nature* **452**, 553–563 (2008).
2. Van Dort, M. E., Rehemtulla, A. & Ross, B. D. PET and SPECT Imaging of Tumor Biology: New Approaches towards Oncology Drug Discovery and Development. Curr. Comput. *Aided Drug Des.* **4**, 46–53 (2008).
3. Garrett, M. D. & Workman, P. Discovering novel chemotherapeutic drugs for the third millennium. *Eur. J. Cancer* **35**, 2010–2030 (1999).
4. Abramson, R. G. *et al.* Complications of targeted drug therapies for solid malignancies: manifestations and mechanisms. *AJR Am J Roentgenol.* **200**, 475–483 (2013).
5. Horak, C. E. *et al.* Biomarker analysis of neoadjuvant doxorubicin/cyclophosphamide followed by ixabepilone or Paclitaxel in early-stage breast cancer. *Clin. Cancer Res.* **19**, 1587–1595 (2013).
6. Waddell, T. & Cunningham, D. Impact of targeted neoadjuvant therapies in the treatment of solid organ tumours. *Br. J. Surg.* **100**, 5–14 (2013).
7. Cornett, D. S., Reyzer, M. L., Chaurand, P. & Caprioli, R. M. MALDI imaging mass spectrometry: molecular snapshots of biochemical systems. *Nat. Methods* **4**, 828–833 (2007).
8. Schwamborn, K. & Caprioli, R. M. Molecular imaging by mass spectrometry--looking beyond classical histology. *Nat. Rev. Cancer* **10**, 639–646 (2010).
9. Castellino, S., Groseclose, M. R. & Wagner, D. MALDI imaging mass spectrometry: bridging biology and chemistry in drug development. *Bioanalysis* **3**, 2427–2441 (2011).
10. Saito, Y. *et al.* Development of imaging mass spectrometry. *Biol. Pharm. Bull.* **35**, 1417–1424 (2012).
11. Lorenz, M., Ovchinnikova, O. S., Kertesz, V. & Van Berkel, G. J. Laser microdissection and atmospheric pressure chemical ionisation mass spectrometry coupled for multimodal imaging. *Rapid Commun Mass Spectrom.* **27**, 1429–1436 (2013).
12. Römpp, A. & Spengler, B. Mass spectrometry imaging with high resolution in mass and space. *Histochem Cell Biol.* **139**, 759–783 (2013).
13. Rowinsky, E. K. *et al.* Phase I and pharmacologic study of paclitaxel and cisplatin with granulocyte colony-stimulating factor: neuromuscular toxicity is dose-limiting. *J. Clin. Oncol.* **11**, 2010–2020 (1993).
14. Hamaguchi, T. *et al.* NK105, a paclitaxel-incorporating micellar nanoparticle formulation, can extend in vivo antitumour activity and reduce the neurotoxicity of paclitaxel. *Br. J. Cancer* **92**, 1240–1246 (2005).
15. Hamaguchi, T. *et al.* A phase I and pharmacokinetic study of NK105, a paclitaxel-incorporating micellar nanoparticle formulation. *Br J Cancer* **97**, 170–176 (2007).
16. Kato, K. *et al.* Phase II study of NK105, a paclitaxel-incorporating micellar nanoparticle, for previously treated advanced or recurrent gastric cancer. *Invest. New Drugs* **30**, 1621–1627 (2012).
17. Matsumura, Y. & Kataoka, K. Preclinical and clinical studies of anticancer agent-incorporating polymer micelles. *Cancer Sci.* **100**, 572–579 (2009).
18. Matsumura, Y. & Maeda, H. A new concept for macromolecular therapeutics in cancer chemotherapy: mechanism of tumoritropic accumulation of proteins and the antitumor agent smancs. *Cancer Res.* **46**, 6387–6392 (1986).
19. Duncan, R. Polymer conjugates as anticancer nanomedicines. *Nat. Rev. Cancer* **6**, 688–701 (2006).
20. Peer, D. *et al.* Nanocarriers as an emerging platform for cancer therapy. *Nat. Nanotechnol.* **2**, 751–760 (2007).
21. Ibrahim, N. K. *et al.* Multicenter phase II trial of ABI-007, an albumin-bound paclitaxel, in women with metastatic breast cancer. *J Clin Oncol.* **23**, 6019–26 (2005).
22. Johnson, D. H., Chang, A. Y. & Ettinger, D. S. Taxol (paclitaxel) in the treatment of lung cancer: the Eastern Cooperative Oncology Group experience. *Ann Oncol.* **Suppl 6**, S45–50 (1994).
23. Matsumura, Y. Cancer stromal targeting (CAST) therapy. *Adv Drug Deliv Rev.* **64**, 710–719 (2012).
24. Dimou, A., Syrigos, K. N. & Saif, M. W. Overcoming the stromal barrier: technologies to optimize drug delivery in pancreatic cancer. *Ther Adv Med Oncol.* **5**, 271–279 (2012).